JOURNAL OF Applied Polymer SCIENCE

Special Issue: Microfiltration and Ultrafiltration Membrane Science and Technology

Guest Editors: Prof. Isabel C. Escobar (University of Toledo) and Prof. Bart Van der Bruggen (University of Leuven)

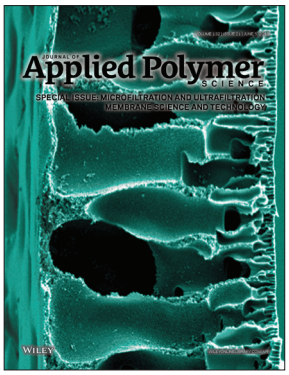

EDITORIAL

Microfiltration and Ultrafiltration Membrane Science and Technology
I. C. Escobar and B. Van der Bruggen, *J. Appl. Polym. Sci.* 2015, **DOI: 10.1002/app.42002**

REVIEWS

Nanoporous membranes generated from self-assembled block polymer precursors: *Quo Vadis*?
Y. Zhang, J. L. Sargent, B. W. Boudouris and W. A. Phillip, *J. Appl. Polym. Sci.* 2015, **DOI: 10.1002/app.41683**

Making polymeric membranes anti-fouling via "grafting from" polymerization of zwitterions
Q. Li, J. Imbrogno, G. Belfort and X.-L. Wang, *J. Appl. Polym. Sci.* 2015, **DOI: 10.1002/app.41781**

Fouling control on MF/ UF membranes: Effect of morphology, hydrophilicity and charge
R. Kumar and A. F. Ismail, *J. Appl. Polym. Sci.* 2015, **DOI: 10.1002/app.42042**

EMERGING MATERIALS AND FABRICATION

Preparation of a poly(phthalazine ether sulfone ketone) membrane with propanedioic acid as an additive and the prediction of its structure
P. Qin, A. Liu and C. Chen, *J. Appl. Polym. Sci.* 2015, **DOI: 10.1002/app.41621**

Preparation and characterization of MOF-PES ultrafiltration membranes
L. Zhai, G. Li, Y. Xu, M. Xiao, S. Wang and Y. Meng, *J. Appl. Polym. Sci.* 2015, **DOI: 10.1002/app.41663**

Tailoring of structures and permeation properties of asymmetric nanocomposite cellulose acetate/silver membranes
A. S. Figueiredo, M. G. Sánchez-Loredo, A. Maurício, M. F. C. Pereira, M. Minhalma and M. N. de Pinho, *J. Appl. Polym. Sci.* 2015, **DOI: 10.1002/app.41796**

LOW-FOULING POLYMERS

Low fouling polysulfone ultrafiltration membrane via click chemistry
Y. Xie, R. Tayouo and S. P. Nunes, *J. Appl. Polym. Sci.* 2015, **DOI: 10.1002/app.41549**

Elucidating membrane surface properties for preventing fouling of bioreactor membranes by surfactin
N. Behary, D. Lecouturier, A. Perwuelz and P. Dhulster, *J. Appl. Polym. Sci.* 2015, **DOI: 10.1002/app.41622**

PVC and PES-*g*-PEGMA blend membranes with improved ultrafiltration performance and fouling resistance
S. Jiang, J. Wang, J. Wu and Y. Chen, *J. Appl. Polym. Sci.* 2015, **DOI: 10.1002/app.41726**

Improved antifouling properties of TiO_2/PVDF nanocomposite membranes in UV coupled ultrafiltration
M. T. Moghadam, G. Lesage, T. Mohammadi, J.-P. Mericq, J. Mendret, M. Heran, C. Faur, S. Brosillon, M. Hemmati and F. Naeimpoor, *J. Appl. Polym. Sci.* 2015, **DOI: 10.1002/app.41731**

Development of functionalized doped carbon nanotube/polysulfone nanofiltration membranes for fouling control
P. Xie, Y. Li and J. Qiu, *J. Appl. Polym. Sci.* 2015, **DOI: 10.1002/app.41835**

JOURNAL OF Applied Polymer SCIENCE

Special Issue: Microfiltration and Ultrafiltration Membrane Science and Technology

Guest Editors: Prof. Isabel C. Escobar (University of Toledo) and
Prof. Bart Van der Bruggen (University of Leuven)

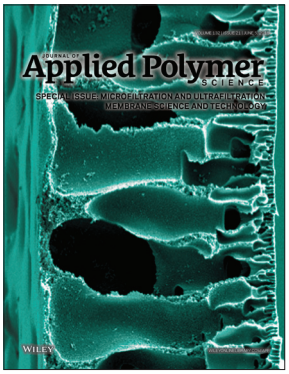

SURFACE MODIFICATION OF POLYMER MEMBRANES

Highly chlorine and oily fouling tolerant membrane surface modifications by *in situ* polymerization of dopamine and poly(ethylene glycol) diacrylate for water treatment
K. Yokwana, N. Gumbi, F. Adams, S. Mhlanga, E. Nxumalo and B. Mamba, *J. Appl. Polym. Sci.* 2015, **DOI: 10.1002/app.41661**

Fouling control through the hydrophilic surface modification of poly(vinylidene fluoride) membranes
H. Jang, D.-H. Song, I.-C. Kim, and Y.-N. Kwon, *J. Appl. Polym. Sci.* 2015, **DOI: 10.1002/app.41712**

Hydroxyl functionalized PVDF-TiO_2 ultrafiltration membrane and its antifouling properties
Y. H. Teow, A. A. Latif, J. K. Lim, H. P. Ngang, L. Y. Susan and B. S. Ooi, *J. Appl. Polym. Sci.* 2015, **DOI: 10.1002/app.41844**

Enhancing the antifouling properties of polysulfone ultrafiltration membranes by the grafting of poly(ethylene glycol) derivatives via surface amidation reactions
H. Yu, Y. Cao, G. Kang, Z. Liu, W. Kuang, J. Liu and M. Zhou, *J. Appl. Polym. Sci.* 2015, **DOI: 10.1002/app.41870**

SEPARATION APPLICATIONS

Experiment and simulation of the simultaneous removal of organic and inorganic contaminants by micellar enhanced ultrafiltration with mixed micelles
A. D. Vibhandik, S. Pawar and K. V. Marathe, *J. Appl. Polym. Sci.* 2015, **DOI: 10.1002/app.41435**

Polymeric membrane modification using SPEEK and bentonite for ultrafiltration of dairy wastewater
A. Pagidi, Y. Lukka Thuyavan, G. Arthanareeswaran, A. F. Ismail, J. Jaafar and D. Paul, *J. Appl. Polym. Sci.* 2015, **DOI: 10.1002/app.41651**

Forensic analysis of degraded polypropylene hollow fibers utilized in microfiltration
X. Lu, P. Shah, S. Maruf, S. Ortiz, T. Hoffard and J. Pellegrino, *J. Appl. Polym. Sci.* 2015, **DOI: 10.1002/app.41553**

A surface-renewal model for constant flux cross-flow microfiltration
S. Jiang and S. G. Chatterjee, *J. Appl. Polym. Sci.* 2015, **DOI: 10.1002/app.41778**

Ultrafiltration of aquatic humic substances through magnetically responsive polysulfone membranes
N. A. Azmi, Q. H. Ng and S. C. Low, *J. Appl. Polym. Sci.* 2015, **DOI: 10.1002/app.41874**

BIOSEPARATIONS APPLICATIONS

Analysis of the effects of electrostatic interactions on protein transport through zwitterionic ultrafiltration membranes using protein charge ladders
M. Hadidi and A. L. Zydney, *J. Appl. Polym. Sci.* 2015, **DOI: 10.1002/app.41540**

Modification of microfiltration membranes by hydrogel impregnation for pDNA purification
P. H. Castilho, T. R. Correia, M. T. Pessoa de Amorim, I. C. Escobar, J. A. Queiroz, I. J. Correia and A. M. Morão, *J. Appl. Polym. Sci.* 2015, **DOI: 10.1002/app.41610**

Hemodialysis membrane surface chemistry as a barrier to lipopolysaccharide transfer
B. Madsen, D. W. Britt, C.-H. Ho, M. Henrie, C. Ford, E. Stroup, B. Maltby, D. Olmstead and M. Andersen, *J. Appl. Polym. Sci.* 2015, **DOI: 10.1002/app.41550**

Membrane adsorbers comprising grafted glycopolymers for targeted lectin binding
H. C. S. Chenette and S. M. Husson, *J. Appl. Polym. Sci.* 2015, **DOI: 10.1002/app.41437**

Journal of Applied Polymer Science

Forensic analysis of degraded polypropylene hollow fibers utilized in microfiltration

Xiaoyun Lu,[1] Parag Shah,[2] Sajjad Maruf,[1] Sean Ortiz,[1] Theresa Hoffard,[3] John Pellegrino[1]

[1]Mechanical Engineering, University of Colorado, Boulder, Colorado 80309

[2]Chemical and Biological Engineering, University of Colorado, Boulder, Colorado 80309

[3]Naval Facilities Engineering and Expeditionary Warfare Center, Port Hueneme, California 93043

Correspondence to: J. Pellegrino (E-mail: john.pellegrino@colorado.edu)

ABSTRACT: Numerous polypropylene hollow fiber microfiltration membrane modules were severely degraded after utilization as pretreatment in a military water purification system. To determine the plausible causes of degradation, thermal, chemical, and mechanical material properties were initially evaluated by using differential scanning calorimetry, thermogravimetric analysis, ^{13}C solid-state nuclear magnetic resonance, attenuated total reflectance infrared spectroscopy, and a tensile strength material testing system. The evaluation implied oxidation during the usage or storage of the samples. Protocols using more specialized techniques, micro-Raman spectroscopy along with energy dispersive X-ray spectroscopy and an atomic force microscope-based nano-thermal analysis, were developed to examine the chemical and thermal properties along the cross-section of the samples at the micron and submicron-scale. These results indicated that the degradation mainly took place at the outer and inner boundaries of the samples. Pristine samples exposed to several plausibly harsh environments did not evidence the same level of mechanical failure, but a few circumstances had similar test responses, leading to a hypothesis of high oxidative stress as the main failure etiology versus a slowly evolving one. © 2014 Wiley Periodicals, Inc. J. Appl. Polym. Sci. **2015**, *132*, 41553.

KEYWORDS: degradation; mechanical properties; membranes; polyolefins

Received 26 June 2014; accepted 19 September 2014

DOI: 10.1002/app.41553

INTRODUCTION

To minimize membrane contamination and flux-decline caused by colloidal and suspended species during reverse osmosis (RO) processes, a prefiltration system utilizing microfiltration (MF) or ultrafiltration (UF) is of great importance for particle removal before the RO step.[1–3] With symmetric pore structure and high specific surface area, polypropylene hollow fibers (PP-HFs) are one of the widely used membranes in MF.[4,5] Polypropylene (PP) is a thermoplastic material that is produced by polymerization of propylene. The polymer chain length and the crystalline structure give PP useful physical, mechanical, thermal, and chemical properties and stability.[6–8] However, the structure, morphology, method of production and in-use environmental factors can greatly affect the service and lifetime of PP and highly influence its degradation characteristics.[9,10] With the existence of tertiary carbon bonds, the polyolefins undergo thermal oxidation in air at elevated temperatures,[11–13] but can also be oxidized slowly in the presence of oxygen or oxidants at ambient temperature. Oxidative-degradation is also accelerated by the presence of certain transition metals, high shear mechanical forces, or ultraviolet irradiation.[14,15]

The complicated PP oxidation mechanism has been studied extensively for the last several decades.[11–13,16] Generally, hydrocarbons are susceptible to oxidation by free-radical chain reaction to form hydroperoxides. Then hydroperoxides can autocatalytically accelerate the oxidation reaction. After oxidation, lower molecular weight molecules containing alcohol, hydroperoxides, or carbonyl groups are formed which have lower thermal and mechanical stability than PP.

In recent years, PP-HFs were deployed as a prefiltration system in a military water purification system. However, numerous modules (over 50%) that returned from the field were severely degraded and could no longer be utilized—see Supporting Information Figure S1. In general, the application duration for the modules was relatively short, varying from 4 days to approximately 2 months. Before deployment, the modules were installed in the system and then stored in warehouses for

Additional Supporting Information may be found in the online version of this article.

Table I. Detailed Information of PP-HF Samples for Failure Analysis Including Manufacturing Date, Operating Hours, Condition of Operation, and Failure Description

Sample no.	Filter module manufacturing date	Operating hours	Comments
1	05/2010	N/A	Pristine sample
2	06/2003	1423.3	Rust stains, not cleaned or preserved. Fiber only elongates 5–10% before break.
3A	04/2007	43.3	One side of the internal of the bundle is severely degraded.
3B	04/2007	43.3	One side of the internal of the bundle is severely degraded.
4A	06/2006	4.3	Very brittle, almost no elongation. Internal of the bundle is severely degraded.
4B	06/2006	4.3	Very brittle, almost no elongation. Internal of the bundle is severely degraded.
5	07/1999	823	5 y of storage/very intermittent operation in a wastewater plant outdoors and 823 h of seawater operations.

different periods of time from several months up to as long as 10 years. This has been normal procedure over many years and modules without incident until the experiences precipitating this study.

We hypothesized that these PP-HFs' degradation could have been due to the existence of oxidant or chlorine in the water resources during usage or an extreme environmental condition such as a high temperature excursion or sunlight (UV) exposure during storage. A variety of materials testing studies have been done on these degraded PP-HF samples including organic solvent solubility, scanning electronic microscopic (SEM) imaging, thermal analysis with differential scanning calorimetry (DSC), thermogravimetric analysis (TGA), chemical analysis with ^{13}C solid-state nuclear magnetic resonance (NMR), and attenuated total reflectance infrared spectroscopy (ATR-IR), and mechanical analysis with, a material testing system (MTS). These measurements confirmed that oxidation was the main cause of the degradation. Nonetheless, the etiology of oxidation was also of interest, so we explored further analytical approaches to obtain more detailed evidence indicating a degradation mechanism and the potential process. While the definitive failure mode is still elusive, and only relevant to the particular application, these methods and interpretations may be useful for any polymer accelerated aging/exposure studies, in general.

Of particular note, methods to study the micron and submicron-scale chemical and thermal properties over the PP-HF wall's cross-section, using micro-Raman spectroscopy along with energy dispersive X-ray spectroscopy (EDS) and an atomic force microscope (AFM) based nano-thermal analysis (nano-TA), were developed and applied.[17,18] The purpose of these studies were to elucidate whether degradation had occurred starting at any particular surface by measuring the variation of the chemical and thermal properties across the cross-section. The analytical results further confirmed oxidative-degradation, and indicated the degradation took place at both the outer and inner boundaries of the samples versus homogeneously throughout.

Pristine samples from the same manufacturer, and from a different one, were also exposed to various controlled conditions meant to mimic harsh, but plausible, environmental excursions. These included varying temperatures (high and low) or being soaked in various chemicals (base or acid) for different time periods. TGA, DSC, and MTS tests were performed and further tests were carried out on some of the samples by ATR-IR. Test results implied that some chemical exposures, temperature variation or samples being dried after wetting could initiate the degradation.

EXPERIMENTAL

Specimens from one pristine (Sample 1) and six degraded samples 2, 3A, 3B, 4A, 4B, and 5 were the primary materials studied. The details of the samples' manufacturing date, operation time, condition of operation, and failure description are listed in Table I.

Bulk Material Studies

Before measurements, the sample specimens were soaked and cleaned with deionized (DI) water to remove impurities from their surface. All of the pristine and used samples were vacuum dried at ambient temperature overnight to achieve uniform initial test conditions. At least three replicate specimens were tested for each sample.

- Initially, solubility of the PP-HFs in p-xylene was measured. ACS grade p-xylene was purchased from Aldrich.
- SEM (JSM-6480LV, Jeol, Japan) was employed for image analysis of the samples' outer surface and cross-section. In addition, EDS (JSM-6480LV, Jeol, Japan) was employed for further elemental analysis on the local microscale area of outer surface, and cross-section.
- Thermal degradation was analyzed by TGA using a TGA (Pyris 1, PerkinElmer, Waltham, MA), and DSC (204F1, Netzsch, Selb, Germany). To avoid oxidation during TGA, measurements were carried out in an inert nitrogen atmosphere with a flow rate of 20 mL/min. Samples were heated from 25 to 800°C at the rate of 10°C/min. DSC analysis was performed with two repeated heating and cooling cycles with a 10°C/min heating rate under nitrogen purge environment in a 25 to 200°C temperature range.

Table II. Summary Results from Bulk Analysis of the PP Fiber Samples

Analytical method	Sample 1	Sample 2	Sample 3 (A&B)	Sample 4 (A&B)	Sample 5
p-xylene solubility at 140°C	Completely soluble	Some insoluble species	Some insoluble species	Some insoluble species	Some insoluble species
SEM	Normal	Physical cracks	Physical cracks	Physical cracks	Physical cracks
NMR	Only PP	Only PP	Peroxides	Peroxides & alcohol	Only PP
ATR-FTIR	Only PP	C—O & C—O—C alcohols	C—O & C—O—C alcohols	C—O & C—O—C alcohols	C—O & C—O—C alcohols
DSC	Baseline	Slightly lower temperature for melting transitions	Lower temperature for melting transitions	Very significant differences than baseline	Slightly differences than baseline
TGA	Mass loss begins at ~275-450°C	Mass loss begins at ~275-500°C	Mass loss begins at ~175-275°C	Mass loss begins at ~100-250°C	Mass loss begins at ~265°C
MTS	1.72 ± 0.03 N break strength	0.99 ± 0.06 N break strength	3A: 1.1 ± 0.09N	4A: 1.16 ± 0.05N	1.32 ± 0.02N break strength
	291 ± 17.9% elongation (baseline value)	62.7 ± 11.9% elongation (much weaker and more brittle)	3B: 0.74 ± 0.16N break strength	4B: 0.42 ± 0.19 N break strength	228.6 ± 15.9% elongation (somewhat weaker and slightly more brittle)
			3A: 113.4 ± 38.4%	4A: 135.8 ± 25.5%	
			3B: 10.6 ± 7% elongation (much weaker and more brittle)	4B: 1.9 ± 0.8% elongation (much weaker and more brittle)	

- The mechanical properties of elongation and maximum load at break were measured using MTS (820.002-SL, Insight II, Eden Prairie, MN). Tests were performed at 25°C with approximately 25 mm fiber lengths and a 250 N load cell and 10 mm/min loading rate.
- Chemical analyses were carried out with solid-state ^{13}C NMR (Varian INOVA-400, Agilent Technologies, Santa Clara, CA) and ATR-IR (FTIR - Nexus 6700, Thermofisher Scientific, Waltham, MA). The NMR spectrometer operates at 100.63 MHz for ^{13}C observation. The probe incorporates a 5 mm Magic Angle Spinning module and coil assembly designed and constructed by Revolution NMR, Inc. (Fort Collins, CO), capable of spinning up to 13 kHz with zirconia rotors (also from Revolution NMR, Inc.) Spectra were acquired using cross-polarization spin-lock and decoupling RF fields of 80.5 kHz, and time-proportional, phase modulation decoupling was applied during signal acquisition. The ATR accessory is a VariGATR grazing angle ATR accessory equipped with a Ge crystal (Harrick Scientific Products, Pleasantville, NY) to identify and quantify the functional groups on the surface of the samples.

Analysis Across the Fiber Wall Cross-Section

Further micron and submicron-scale chemical and thermal analysis of microtomed cross-sections was conducted with micro-Raman spectroscopy and an AFM-based (Bruker DI3100, Billerica, MA) nano-TA (Anasys, Santa Barbara, CA). A cryostat microtome (Leica CM1850, Leica Microsystems, Buffalo Grove, IL) was used to prepare cross-section samples. PP-HF samples in ~1 cm length were embedded vertically in Tissue-Tek® O.C.T. compound (Sakura Finetek, Torrance, CA) in a disposable plastic Tissue-Tek standard cryomold (4557, 25 × 20 × 5 mm, Sakura Finetek, Torrance, CA). Then the embedding medium containing PP-HF samples was quickly frozen in a dry ice box. Once the sample was frozen, it was removed from the cryomold and then mounted on the round metallic mount of the cryostat vertically with Tissue-Tek O.C.T. at a temperature of −20°C. With this orientation, the blade cut parallel to the cross-section of samples. After sectioning, the samples were glued vertically to a microscope glass slide with epoxy hot glue.

The Raman spectra, in the range of 4000–500 cm^{-1} Raman shift, were obtained on a Horiba Scientific U1000 microprobe spectrometer (Horiba Scientific, Edison, NJ). The main elements of the spectrometer are an Olympus BX40 microscope, a single diffraction grating, and an electrically cooled, charge-coupled device camera. Eight Raman scans on the cross-section of each HF sample from the outer to inner boundary at approximately 15 μm spacing was performed.

Nano-TA is an AFM based thermo-mechanical analytical technique, recently introduced by Anasys. With the help of additional

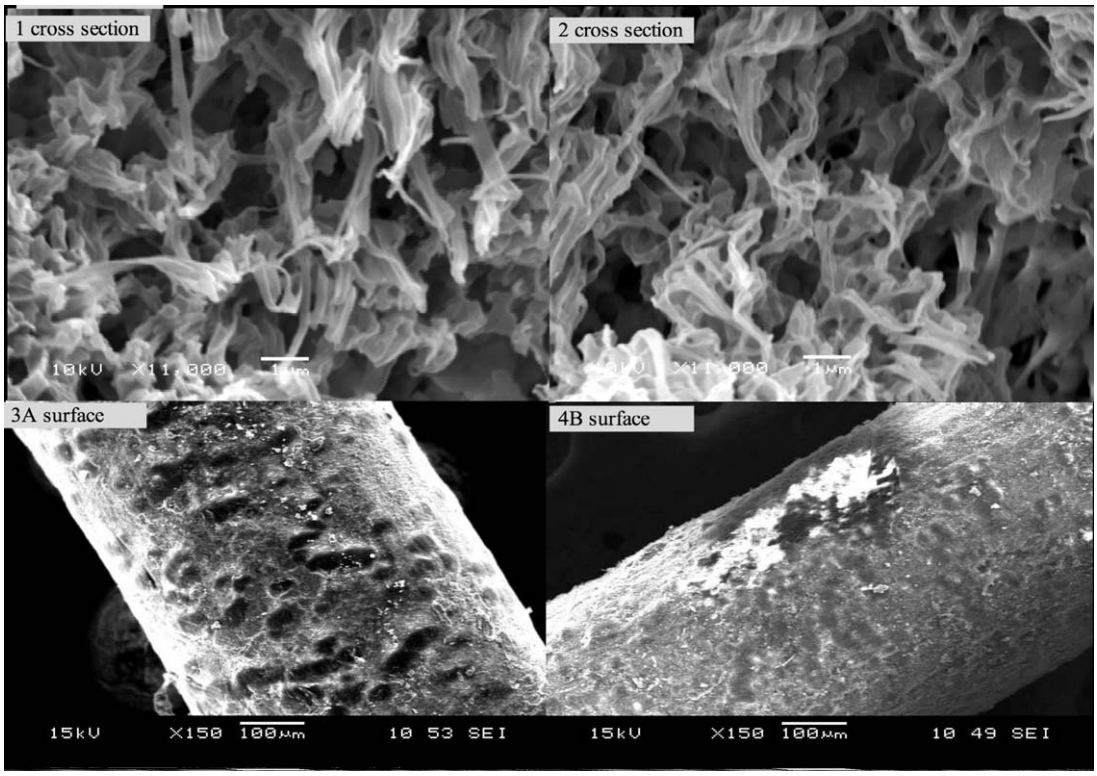

Figure 1. Scanning electron microscope images of cross-section and outer surface of the pristine samples and some degraded polypropylene HF samples.

accessories this technique enables an AFM to measure a material's thermal properties in a sub-100 nm localized area.[19,20] Using the optical resolution of the AFM, a specially manufactured doped silicon probe with tip radius < 30 nm is put in contact at a desired location and heated at a rapid heating rate. These probes have a heater integrated into the end of the cantilever which enables them to be heated in a controlled fashion to 400°C. At the initial stage of each measurement, sample deflection increases with expansion of the sample. When the probe temperature reaches softening temperature of the sample (melting temperature for semi-crystalline polymers and glass transition temperature for amorphous ones), the thermal probe penetrates into the material so sample deflection decreases sharply (see Supporting Information Figure S2). By using this method, the material melting temperature at a localized area can be analyzed and effective distribution/sampling can also be obtained from the controlled lateral displacement after each measurement. In this study, we utilized a custom-made thermal lever probe AN2–200 µm. Each measurement was carried out across the cross-section surface from inner surface to outside boundary for every 15-µm interval. A heating rate of 2°C/s (120°C/min) was used for all the measurements. The measurement temperature range was 25–200°C.

RESULTS AND DISCUSSION

A summary of the results and general conclusions from the bulk material measurements are presented in Table II.

Organic Solvent Solubility Study

PP can be dissolved in a few organic solvents at elevated temperatures.[21–24] While the pristine sample 1 was completely dissolved in p-xylene at ~140°C, all the used samples had varying amounts of insoluble impurities after vigorous mixing (see Supporting Information Figure S3). This result implied chemical degradation products insoluble in p-xylene may exist in these samples. Complete separation, at the elevated temperature, of the insoluble impurities and the dissolved PP was not attempted in this work.

SEM Images

Some illustrative SEM photos are shown in Figure 1. SEM images showed cracks on the outer surface and cross-section of the used samples, while the pristine sample appeared more uniform. In addition, larger and irregular pore shapes were observed in the cross-section image of the used samples. The cracks on the fiber surface and the larger and irregular pores illustrate the material failure under normal end-use conditions that may be related to the chemical changes.

Thermal Property Measurements

Bulk thermal properties were studied with TGA and DSC. TGA measurement results are shown in Figure 2(a). During TGA measurement, there was some initial mass loss due to volatiles, such as water, and then further mass loss (degradation) occurred with increasing temperature. Mass loss for all the used samples (except sample 2), and especially the most degraded ones 3B and 4B, started at significantly lower temperatures compared with the pristine sample. The mass loss of the pristine sample 1 starts at ~350°C while it starts at ~150°C for samples 3B and 4B. The onset temperature and %mass loss for all samples can be found in Supporting Information Table SII.

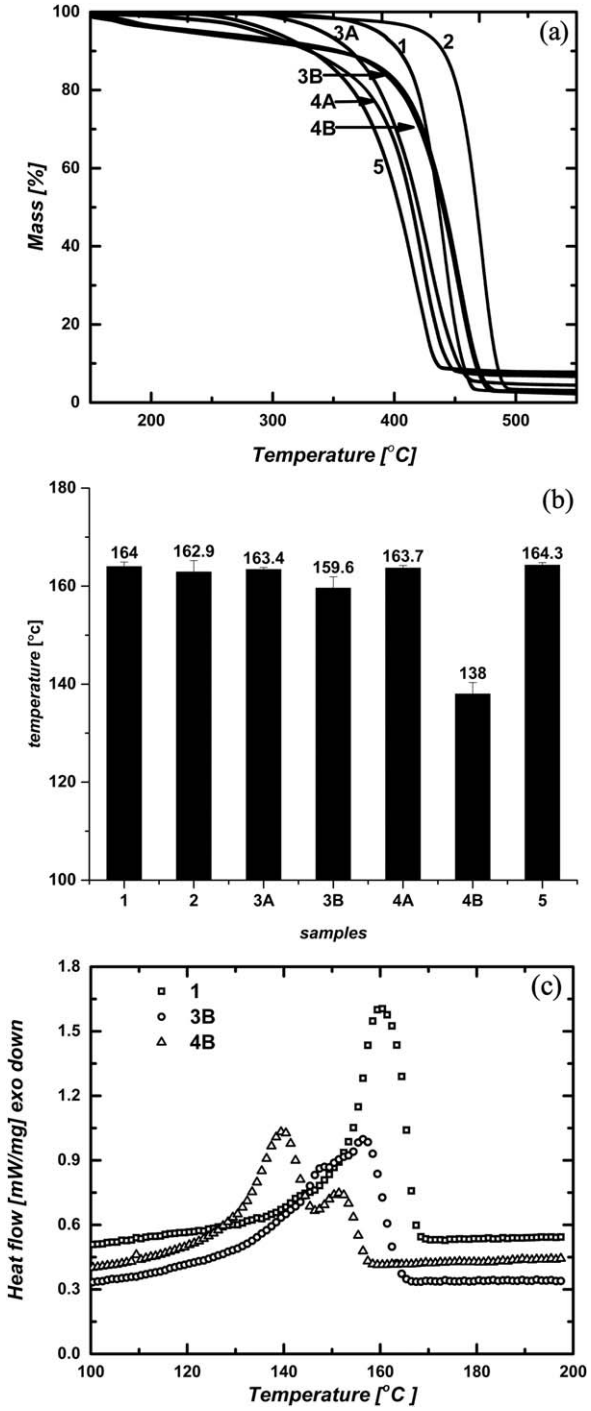

Figure 2. TGA and DSC measurements results for pristine sample 1 and all the degraded samples: (a) mass loss vs. temperature in TGA measurements; (b) melting temperature of all the samples during DSC measurements; (c) the second heating cycle profiles for samples 1, 3B, and 4B.

The particular tested specimens of sample 2 actually indicated a somewhat higher thermal stability than the other used samples. This may be due to these specimens having lower porosity thus lowering the rate of the pyrolysis reaction versus the heating rate. In any case, all measurements were done at least in triplicate with separate specimens, so we are confident in the data. A certain level of inconsistency between a single characterization technique and the macroscopic mechanical properties may be expected, which is why we combined several methods in this study's protocol.

In general, the degraded samples showed significantly lower thermal stability than the pristine fiber. These results indicate that relatively low molecular mass or other volatile products existed in the degraded samples. The volatile products are likely the result of the oxidative-degradation process since the sample preparation (DI water soaking and rinsing) would have removed any materials accumulated during the end-use filtrations.

For DSC analysis, melting temperatures of all samples are summarized in Figure 2(b) (with further detailed data in Supporting Information Table SII) and representative DSC analysis profiles for samples 1, 3B and 4B are shown in Figure 2(c). While the melting temperatures for most of the used samples are only ~1 to 3% lower than that of the pristine sample, the melting temperatures for sample 4B is significantly lower (~14%). In addition, the heating cycle for sample 3B showed a broader peak and two obvious peaks showed up for sample 4B. The lower melting temperature, broader peak and multiple peaks in the heating cycle indicated that possible multiple crystalline species, broader molecular mass distribution of molecules, and/or different chemical entities are present in the degraded samples.[25]

Mechanical Property Measurements

All the degraded samples, especially samples 3B and 4B, had significant decreases in percent elongation at break. Pristine sample 1 had approximately 300% elongation at break, while most of the degraded samples had less than 100%. Most significantly, samples 3B and 4B had almost no elongation before break. In addition, the maximum load at break for the degraded samples also decreased dramatically. For most of the samples, it decreased ~ 30 to 40%, while it decreased 57% for sample 3B and 76% for sample 4B. The dramatic decreases of percent elongation and maximum load indicated that all the used samples have degraded in a certain degree. The average value of

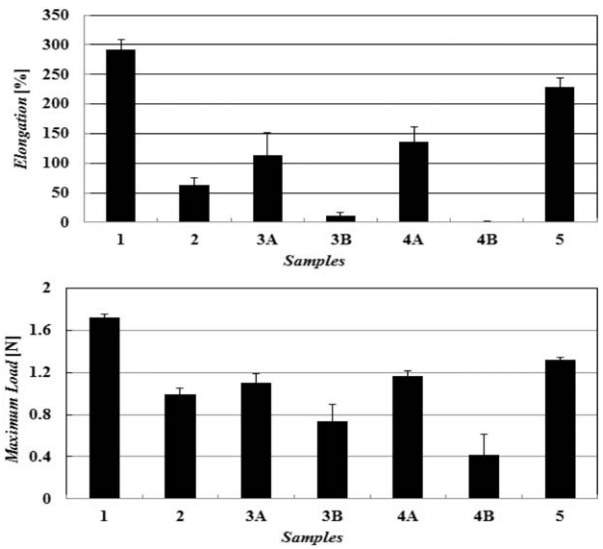

Figure 3. MTS measurements results with percent elongation and maximum load at break for all the samples.

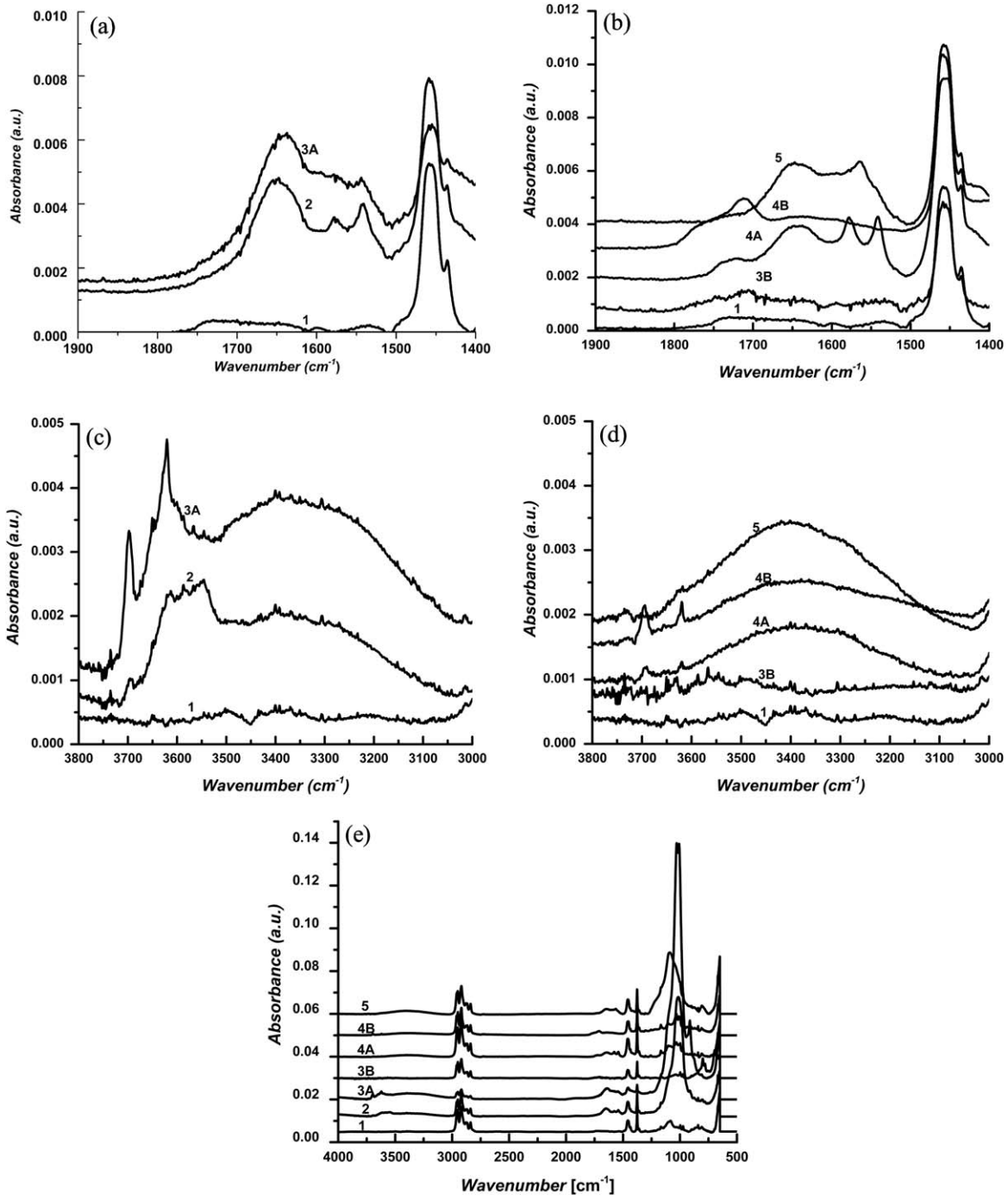

Figure 4. ATR-IR spectra the samples. Two regions of interest at 1400–1900 cm^{-1} and 3000–3800 cm^{-1} were enlarged for easier observation. (a) In region 1400–1900 cm^{-1}, the spectra are grouped corresponding to (a) samples 1, 2, and 3A and (b) samples 1, 3B, 4A, 4B, and 5 from bottom to top, respectively. In region 3000–3800 cm^{-1}, grouped corresponding to (c) samples 1, 2, and 3A and (d) samples 1, 3B, 4A, 4B, and 5 from bottom to top, respectively. (e) The full scan is shown and spectra were stacked up in the order of samples 1, 2, 3A, 3B, 4A, 4B, and 5 from bottom to top, respectively.

percent elongation and maximum load at break for all the samples are summarized in Figure 3.

Chemical Analysis

^{13}C NMR spectra for all the samples have three peaks at chemical shifts ~21, 26, and 44 ppm which correspond to the PP backbone. Samples 3B, 4A, and 4B showed an extra peak at chemical shift ~85 to 86 ppm which corresponds to hydroperoxides or dialkyl peroxide. Sample 4B showed another extra peak at ~74 ppm which corresponds to tertiary alcohol.[11,13] No obvious additional peaks were observed with the other degraded samples, but this is likely due to sampling heterogeneity and the need for further method development. NMR profiles of all the samples are in the attached Supporting Information in Figure S4.

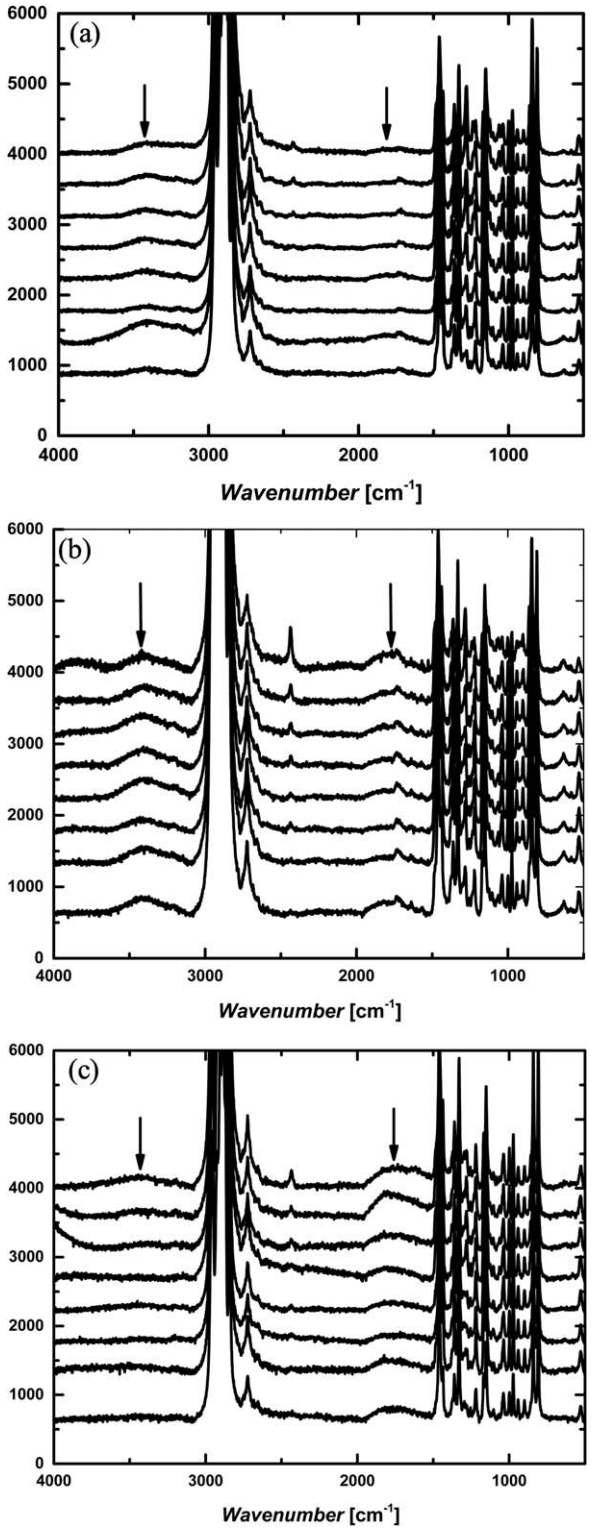

Figure 5. Representative Raman spectra of (a) sample 1; (b) sample 4A; and (c) sample 4B. Raman spectra for other samples can be found in the supplemental information. The spectra are stacked up for easy observation. Eight scans on the cross-section of each HF sample from the outer to inner boundary at approximately 15-μm spacing were performed. The top spectrum is for scan at the outermost boundary. Arrows indicate peaks of main interest (vertical axis is arbitrary units).

Prior studies[11,16] have indicated that hydroperoxide is one of the initial products during radical oxidation of PP and it plays an important role in further oxidation. Findings in the NMR measurements indicated that oxidation has indeed occurred and peroxides are present consistently with free-radical chain reaction.

To further investigate the chemical alteration, ATR-IR was utilized to identify the chemical entities on the sample's bulk outer surface. ATR-IR analysis spectra are shown in Figure 4. The broad peaks observed between 3700 cm^{-1} and 3000 cm^{-1} are due to the —OH stretching vibrations.[26,27] Most of the degraded samples showed an absorption band in this region. These results indicate that alcohols and hydroperoxides formed in the degraded PP samples.

The region between 1750 cm^{-1} and 1500 cm^{-1} showed differences in the ATR-IR spectra for most of the samples. This region is the carbonyl region and the broad bands of most of the samples show that these samples may be a mixture of aldehydes, ketones, carboxylic acids and esters. All the degraded samples have two peaks in common; at 1650 cm^{-1} and 1550 cm^{-1}. Samples 3B and 4B have a small peak at around 1700 cm^{-1}, which could be a carboxylic acid monomer or dimer. Since this peak is evident only for samples 3B and 4B, it shows that these samples are in a more advanced state of oxidation than the other ones.

In addition, sample 5 shows a strong peak around 1100 cm^{-1} and that could be due to secondary or tertiary alcohols. Samples 2 and 3A show a strong band around 1000 cm^{-1} and that could be due to primary alcohol. It should be noted that these bands for all the samples are broad and so, as expected, all of them appear to have a mixture of alcohols to varying degrees since alcohols are well-recognized as products in the propagation of free-radical degradation of PP.[26]

Further Chemical Analysis: Micro-Raman Spectroscopy and EDS

NMR and ATR-IR results indicated that the samples had certainly experienced oxidation. However, the results only reflect an average or sum of the changes across the bulk samples. To further investigate the chemical changes and possible mechanism of oxidation, micro-Raman spectroscopy was utilized to study the microscale chemical signals across the samples' cross-section.

Raman spectra along the cross-section of representative samples are shown in Figure 5 and the rest can be found in the Supplemental Information in Figure S5. The spectra are stacked for easy comparison with the most outer boundary (outside diameter of the fiber) spectrum at the top. Comparing with pristine sample 1, a new peak at ~1740 cm^{-1} was observed for all the degraded samples. This peak corresponds to carbonyl —C═O aldehyde stretching groups.[27–31] Another peak at ~3450 cm^{-1} which is due to —OH bond was observed for some of the samples but is not evident in all of them. This is consistent with the findings in NMR and ATR-IR measurements. In addition, the oxidation peaks for most of the samples only showed up in

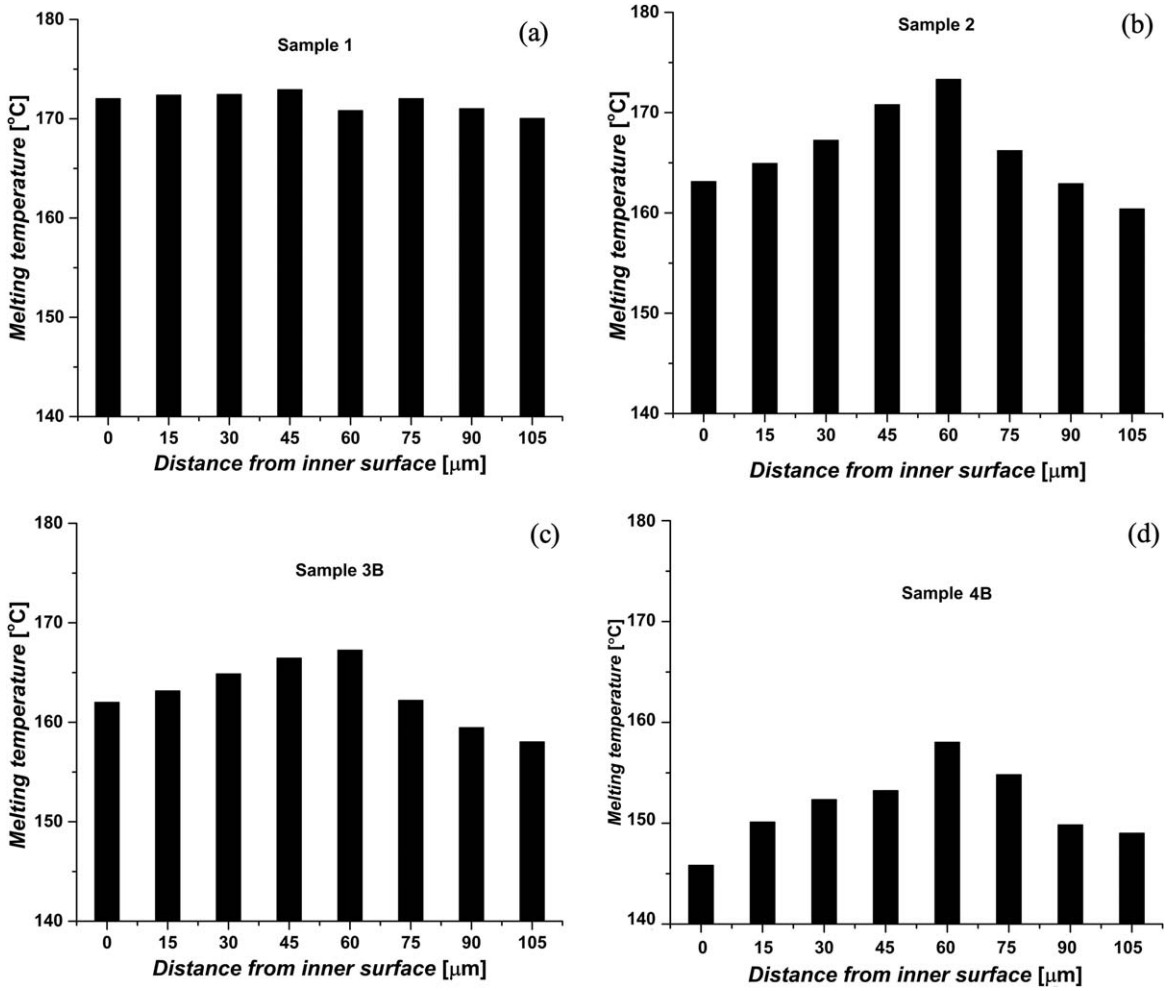

Figure 6. Nano-TA melting temperature results from outer to inner surfaces of the cross-section of (a) pristine sample 1 and the degraded samples 2, 3B, and 4B (labeled b, c, and d, respectively).

the first few scans and the last couple of scans, which corresponded to the outer and inner boundaries, respectively.

Additional analysis using EDS to determine the elements on the outer surface and cross-section of each sample was performed. About 10–30% of oxygen was detected on the cross-section of the samples while ~20–50% of oxygen was detected on the outer surface. This result confirms the oxidation of the samples, and further indicates that the outer surface is more significantly degraded. The EDS study results can be found in the Supporting Information Figure S6 and Table SIII.

Further Thermal Analysis: Nano-TA

Further thermal analysis in submicron scale area was performed with nano-TA. Representative nano-TA study results are shown in Figure 6 (with other results in Supporting Information Figure S7). For pristine sample 1, the melting temperatures from outer to inner surfaces are consistent with an average value of 171.7 ± 1.0°C. Note that, the bulk melting temperature of PP was previously determined to be 164°C which is somewhat lower than the melting temperature obtained via nano-TA. It is well documented that the melting temperature value obtained by a given method depends on the heating or cooling rate applied. Melting temperature is a kinetic event and it is highly dependent on temperature and time. The transition will shift to a higher temperature when heated at a higher heating rate as it has less time at any specific temperature.[32] The nano-TA measurements utilized a heating rate of 120°C/min. This is six times higher than the heating rate employed in the DSC and minimizes the lateral drift of the AFM probe, which becomes noticeable at lower heating rates. However, DSC measurements on the PP samples could not employ such a relatively high rate due to limitation in the instrument capability. One co-author from this paper also found this similar difference in other polymer's transition temperature measured with DSC and nano-TA.[19]

In these measurements, all the degraded samples showed an obvious trend toward lower melting temperatures at the outer and inner boundaries compared with the center of the HF wall. Sample 2 and 3B had lower melting temperatures at the outer boundary than the inner boundary while other samples showed similar values at both of the boundaries. Samples 3B and 4B had the most significant decrease in melting temperature indicating severe degradation. These testing results indicated that the degradation occurred mostly at the boundaries (mostly the outer boundary) and gradually moved through the wall

Table III. Controlled Environmental Exposures of Pristine PP HF Samples with Mechanical Testing Results (Italics Indicate Samples with Significant Change)

Sample no.	Description	Elongation (%)	Max. load (N)
1	Pristine fiber used for 3-# controlled exposures	291.1 ± 17.9	1.72 ± 0.03
3-1	Soaked in DI water for 30 days	291.3 ± 22.7	1.73 ± 0.07
3-2	Soaked in DI water overnight then placed in an open tube in 71°C oven for 30 days. Water was allowed to evaporate to dry out the strands	278.8 ± 85.2	*1.47 ± 0.09*
3-3	Soaked in DI water overnight then placed in a sealed glass tube to retain water in a 71°C oven for 30 days	284.8 ± 9.2	1.68 ± 0.02
3-4	Soaked in 2.3% Tergajet (A commercial high pH, low phosphate detergent) overnight and placed in a sealed glass tube in a 71°C oven for 30 days	*222.4 ± 59.7*	1.66± 0.09
3-5	Soaked in 0.8% NaOH solution and placed in a sealed glass tube in a 71°C oven for 30 days	238.4 ± 48.7	1.63 ± 0.09
3-6	Soaked in 1% sodium meta-bisulfite $Na_2S_5O_5$, (pH 4.3) for 30 days	256.6 ± 18.3	1.57 ± 0.01
3-7	Soaked in 10 ppm free chlorine Cl_2 for 30 days	*84.5 ± 33.1*	*1.22 ± 0.21*
3-8	−10°C/+10°C freeze thaw	296.0 ± 28.7	1.67 ± 0.02
3-9	−10°C/+10°C freeze thaw in a closed tube with water vapor after soaking in DI water overnight	315.6 ± 78.5	1.65 ± 0.06
3-10	−10°C/+10°C freeze thaw after overnight in 2.3% Tergajet	397 ± 115.3	1.54 ± 0.27
3-11	−10°C/+10°C freeze thaw after overnight in 0.8% NaOH	337.4 ± 59.6	1.69± 0.01
2	Pristine fiber used for 4-# controlled exposures	75.5 ± 31.4	5.81 ± 2.97
4-1	Soaked in DI water for 30 days	64.4 ± 4.4	3.23 ± 0.11
4-2	Soaked in DI water overnight then placed in an open tube in a 71°C oven for 30 days, water was allowed to evaporate to dry out the strands	70.9 ± 4.1	5.58 ± 0.71
4-3	Soaked in 1% sodium meta-bisulfite $Na_2S_5O_5$, for 30 days	61.5 ± 22.9	7.19 ± 0.75
4-4	Soaked in 10 ppm free chlorine Cl_2 for 30 days	84.0 ± 0.9	7.66 ± 1.39
4-5	−10°C/+10°C freeze thaw	*40.7 ± 33.0*	6.03 ± 1.14

thickness. In addition, the melting temperatures for the center of most of the samples (except 3B and 4B) are very close to that of pristine sample 1. This result implies that the center of the samples is intact or only slightly degraded. It should be noted that these membranes are selective toward colloids and particles sized ~200 nm and above. Thus, any chemical exposure is expected to fully permeate its porous structure.

Controlled Environmental Exposure Tests

To further investigate the possible etiology of degradation, pristine sample 1 and pristine sample 2-1, which was provided by an alternative manufacturer, were treated under various harsh environments including temperature variation, being dried up after wetting, soaking in different oxidizing chemicals, or a combination of these conditions. The conditions were chosen to represent excursions from normal protocols including cleaning and storage. For example, 10 ppm free chlorine was used as an extreme oxidizing exposure since it is 10 to 20× the residual chlorine level for drinking water, which may have been introduced into the membrane modules before storage. The detailed environmental exposure information and the resulting mechanical test data can be found in Table III.

Thermal and mechanical properties of each sample were first measured using DSC (see Supporting Information Table SIV), TGA (see Supporting Information Figures S9 and S10), and MTS (see Supporting Information Table SV). Then the samples which exhibited diminished thermal or mechanical properties were evaluated with ATR-IR (see Supporting Information Figure S11). Samples of pristine Sample 1 exposed to strong acid or base, free chlorine, temperature variation, or stored dried up after wetting, showed varying levels of degradation. Samples of pristine sample 2–1, exposed to temperature variations and sample stored dried up after wetting also showed some degraded properties. Interestingly, no degradation was observed for sample 2–1 after soaking in free chlorine. However, under no circumstances was the degradation as severe for these samples in controlled exposure tests as for the six degraded samples from the field. Clearly, additional systematic research is needed to identify suitable controlled, accelerated exposure studies for the original field, end-use conditions.

Without the complete details about how the various membrane modules "existed" over their entire life it is impossible to state with complete certainty what caused the samples to become compromised and thus reach the level of severe degradation that was observed. During manufacturing, high temperature

extrusion could cause initial thermal degradation mostly at the fiber surface boundaries.[33–35] Trace amount of metal catalyst residue or additive of hydroperoxide to control the molecular mass during manufacturing could also accelerate oxidation.[36] During packing, storage and utilization, the oxygen, diffusion-controlled degradation might cause oxidation mostly on the surface boundaries and irradiation from sunlight would certainly degrade the fibers mainly on the outer surface.[10,12] It should be noted that the filtration process was an outside-in process, but impurities in water resources, such as, free chlorine or oxidants, trace amount of metal etc., which could also cause oxidation, should permeate freely though the membrane's porous structure.

CONCLUSIONS

An autopsy of samples of PP-HF membranes utilized as prefiltration in a military water purification system was conducted and compared with a pristine sample. Systematic studies including solubility, SEM images, and thermal, chemical, and mechanical properties for the possible failure causes of multiple of these PP-HFs have been performed. All the degraded samples showed less thermal and mechanical stability, and chemical analysis indicated that oxidation was the main mode of degradation.

Novel material property analysis methods, micro-Raman spectroscopy and nano-TA, were developed to analyze some properties on the micron to submicron scale over the samples' cross-section. This study indicated that the degradation is mainly at the outer and inner diameter of the HF samples, with degradation on the outer wall most consistently observed. These results support a working hypothesis that the oxidative-degradation is consistent with large thermal excursions experienced during deployment and storage, which accelerated any oxidative reactions previously initiated by other manufacturing and end-use exposures.

Pristine samples from the same manufacturer and an alternative manufacturer were exposed to various harsh environments and evaluated. These accelerated exposure studies failed to produce the extent of property degradation found in the original field samples. Nonetheless, strong acid or base, free chlorine, temperature variation, or storage dried up after wetting did cause some degradation.

Exposure to sunlight (and other irradiation), as well as high excursions in environmental temperature should be avoided during storage, shipping, and usage.

ACKNOWLEDGMENTS

The authors acknowledge the University Partnerships Team, U.S. Army Tank Automotive Research, Development, and Engineering Center (TARDEC) for support of this work. Also, Dr. Richard Shoemaker facilitated NMR analysis.

REFERENCES

1. Kumar, M.; Adham, S. S.; Pearce, W. R. *Environ. Sci. Technol.* **2006**, *40*, 2037.
2. Kwon, D. Y.; Vigneswaran, S.; Ngo, H. H.; Shin, H. S. *Water Sci. Technol.* **1997**, *36*, 267.
3. Garin, D.; Fuchs, F.; Crance, J. M.; Deloince, R.; Aymard, M.; Bartoli, M. *Environ. Technol.* **1993**, *14*, 397.
4. Phuntsho, S.; Listowski, A.; Shon, H. K.; Le-clech, P.; Vigneswaran, S. *Desalination* **2011**, *271*, 241.
5. Gryta, M. *J. Membr. Sci.* **2007**. *287*, 67.
6. Polypropylene, Available at: http://en.wikipedia.org/wiki/Polypropylene, Retrieved November 05, 2013.
7. Frank, H. P. In Polypropylene; Morawetz, H., Eds.; Gordon and Breach, Science Publishers, Inc.: New York, **1968**; Chapter *2–3*, pp 10–29, Chapter 5, p 86.
8. Karian, H. G., Ed. In Handbook of Polypropylene and Polypropylene Composites, 2nd ed.; Marcel Dekker Inc.: New York, **2003**; Chapter *2*, p 11.
9. Maier, C.; Calafut, T. In Polypropylene—the Definitive User's Guide and Databook; Plastics Design Library: New York, **1998**; Chapter *2–3*, p 11.
10. Lacoste, J.; Vaillant, D.; Carlsson, D. J. *J. Polym. Sci. Polym. Chem.* **1993**, *31*, 715.
11. Mowery, D. M.; Assink, R. A.; Derson, D. K.; Klamo, S. B.; Berstein, R.; Clough, R. L. *Radiat. Phys. Chem.* **2007**, *76*, 864.
12. Carlsson, D. J.; Garton, A.; Wiles, D. M. *Macromolecules* **1976**, *9*, 695.
13. Mowery, D. M.; Assink, R. A.; Derzon, D. K.; Klamo, S. B.; Clough, R. L.; Bernstein, R. *Macromolecules* **2005**, *38*, 5035–5046.
14. Garcia-Montelongo, X. L.; Martinez-de la Cruz, A.; Vazquez-Rodriguez, S.; Torres-Martinez, Leticia, M. *Mater. Res. Bull.* **2014**, *51*, 56.
15. Ohtani, B.; Adzuma, S.; Miyadzu, H.; Nishimoto, S.; Kagiya, T. *Polym. Degrad. Stab.* **1989**, *23*, 271.
16. Butler, C. H.; Whitmore, P. M. *Polym. Degrad. Stab.* **2013**, *98*, 471.
17. Davies, R. J.; Burghammer, M.; Riekel, C. *Macromolecules* **2008**, *41*, 7251.
18. Maruf, S. H.; Ahn, D. U.; Pellegrino, J.; Killgore, J. P.; Greenberg, A. R.; Ding, Y. *J. Membr. Sci.* **2012**, *405*, 167.
19. Maruf, S. H.; Ahn, D. U.; Greenberg, A. R.; Ding, Y. *Polymer* **2011**, *52*, 2643.
20. Yang, F.; Wornyo, E.; Gall, K.; King, W. P. *Scanning* **2008**, *30*, 197.
21. Macko, T.; Pasch, H.; Milonijc, S. K.; Hiller, W. *Chromatographia* **2006**, *64*, 183.
22. Westerman, L. *J. Polym. Sci. A. Polym. Chem.* **1963**, *1*, 411.
23. Davis, T. E.; Tobias, R. L. *J. Polym. Sci.* **1961**, *1*, 227.
24. Vaughan, M. F.; Francis, M. A. *J. Appl. Polym. Sci.* **1977**, *21*, 2409.
25. Paukkeri, R.; Lehtinen, A. *Polymer* **1993**, *34*, 4083.

26. Rosa, D. S.; Angelini, J. M. G.; Agnelli, J. A. M.; Mei, L. H. I. *Polym. Test.* **2005**, *24*, 1022.
27. Lin-Vien, D.; Colthup, N. B.; Fateley, W. G.; Grasselli, J. G. In The Handbook of Infrared and Raman Characteristic Frequencies of Organic Molecules; Academic Press, Inc.: San Diego, **1991**; Chapter *5–6*, p 61.
28. Infrared Spectroscopy Absorption Table, Available at: http://www.ochemonline.com/Infrared_spectroscopy_absorption_table, Retrieved April 24, 2014.
29. Workman, J. Jr. In Handbook of Organic Compounds, NIR, IR, Raman, and UV-Vis Spectra Featuring Polymers and Surfactants, Vol. 3, IR and Raman spectra; Academic Press: San Diego, **2001**; p 97.
30. Mayo, D. W.; Miller, F. A.; Hannah, R. W., Eds. In Course Notes on the Interpretation of IR & Raman Spectra; John Wiley & Sons Inc., **2004**; Chapter *10*, p 261.
31. Raman Spectroscopy for Analysis and Monitoring, Available at: http://www.horiba.com/fileadmin/uploads/Scientific/Documents/Raman/bands.pdf, Retrieved April 29, 2014.
32. Thomas, L. C. *Am. Lab.* **2001**, *33*, 26.
33. Wilson, J. E. *J. Chem. Phys.* **1954**, *22*, 334.
34. Yang, Y.; Wan, L.; Xu, Z. *J. Membr. Sci.* **2009**, *326*, 372.
35. Iring, M.; Tudos, F. *Prog. Polym. Sci.* **1990**, *15*, 217.
36. Gijsman, P.; Hennekens, J.; Vincent, J. *Polym. Degrad. Stab.* **1993**, *39*, 271.